doi: 10.82124/CEAS-GNC-2026-070 CEAS-GNC-2026-070

Evaluation of an Energy Management System for a Hybrid DC Microgrid Coupled to Ground-Generation Airborne Wind Energy

César Eduardo Perdomo Díaz — Researcher, Electrical Engineering Department Universidad Carlos III de Madrid, Madrid, Spain. ce.perdomodiaz@gmail.com

Gabriel Brondel Oñate — Researcher, Electrical Engineering Department Universidad Carlos III de Madrid, Madrid, Spain. gabriel.brondel@gmail.com

Pablo Flores Martín — Researcher, Electrical Engineering Department Universidad Carlos III de Madrid, Madrid, Spain. pabfloresmartin@gmail.com

Carolina Nicolás Martín — Assistant Professor, Electrical Engineering Department Universidad Carlos III de Madrid, Madrid, Spain. canicola@ing.uc3m.es

Osmany Pérez Ramón Aballe — Researcher, Electrical Engineering Department Universidad de Moa, Cuba. aballeperez83@gmail.com

David Santos Martín — Associate Professor, Electrical Engineering Department Universidad Carlos III de Madrid, Madrid, Spain. dsmartin@ing.uc3m.es

ABSTRACT

Airborne Wind Energy Systems (AWES) can access stronger, steadier high-altitude winds with lower structural and economic requirements than conventional turbines, but their cyclic reel out-/in operation produces highly dynamic power swings that complicate grid integration. This work presents an Energy Management System (EMS) tailored for a ground-generation AWES hybrid microgrid and validates it under variable wind conditions to approximate real environmental dynamics. The EMS implementation is achieved through a state-based controller in MATLAB/Simulink, using Stateflow, that coordinates grid export, a supercapacitor bank, and a battery. A Software-in-the-Loop (SiL) framework models power converters, hybrid electrical storage, and the electric machine while injecting time-varying wind-driven AWES power profiles and prediction uncertainty. Results show that, despite stochastic changes in cycle energy and intra-cycle fluctuations, the EMS maintains DC-bus stability, smooths the power profile delivered to the grid, and minimizes battery cycling by prioritizing supercapacitor action, thereby demonstrating robust operation and effective control under realistic conditions. These findings indicate that variable-wind-aware EMS design is key to dependable AWES integration in decentralized grids and provides a scalable pathway from simulation toward laboratory and field deployment.

Keywords: Airborne Wind Energy, Energy Management System, DC Microgrid, Hybrid Storage, Simulation, Stateflow, Variable Wind

1 Introduction

Airborne Wind Energy Systems (AWES) aim to harvest stronger and often more persistent winds at altitudes that are difficult to access with conventional tower-based turbines [1–3]. In ground-generation AWES, a tethered kite flies crosswind trajectories and transfers traction through the tether to a ground-based winch-generator set. The pumping principle alternates a traction phase, during which energy is extracted, with a retraction phase, during which part of that energy is spent to recover the tether [1, 4]. Figure 1 summarizes the working principle of the technology considered in this paper.

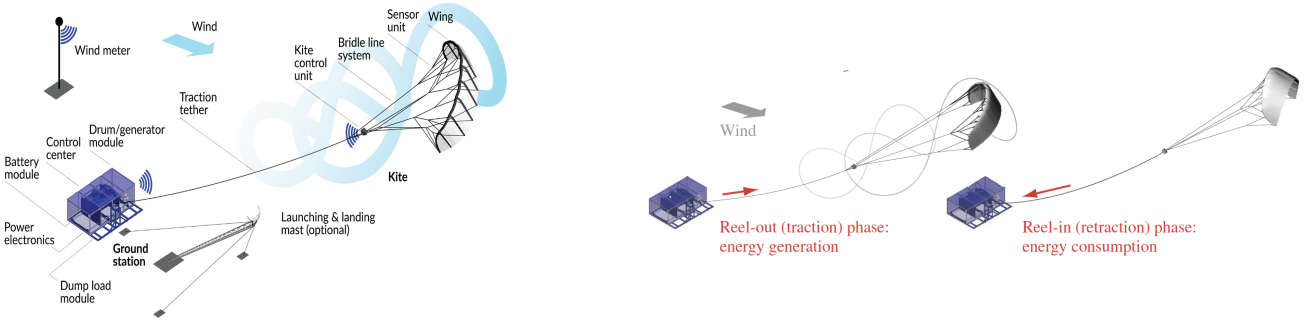

(a) Ground-generation AWES concept. Adapted from [5].

(b) Pumping-cycle principle. Adapted from [6].

Fig. 1 Ground-generation AWES and pumping-cycle operating principle.

At the ground station, the instantaneous mechanical power exchanged by the AWES is governed by the product of tether force, T and reeling speed, v,

$$P_{\text{AWES}} = T\,v, \tag{1}$$

so changes in aerodynamic loading, path geometry, wind conditions, and actuation are transferred directly to the electrical interface [4, 7]. As a result, the source seen by the DC bus is not quasi-steady. It contains fast intra-cycle fluctuations associated with the figure-eight maneuver and slower cycle-to-cycle changes in net energy. Direct grid export therefore requires an intermediate energy-management layer capable of buffering short-term power excursions while correcting longer-term energy imbalance.

Hybrid storage is a natural candidate for this task because the relevant physical time scales are separated. A supercapacitor can absorb fast power swings with limited energy content, while a battery is better suited to slower corrective action [8, 9]. For AWES, however, the relevant input to the EMS is not a generic renewable fluctuation but a profile shaped by coupled flight dynamics, reeling kinematics, and actuation. An EMS evaluation that relies only on nominal or idealized pumping cycles is therefore incomplete.

This paper focuses on that missing step. It presents a simulation-based evaluation of a Stateflow EMS for a hybrid DC microgrid supplied by a ground-generation AWES. Variable pumping-cycle profiles are generated with the LAKSA/KiteAcrobat environment [10, 11] and injected into a Software-in-the-Loop electrical model.

2 Related Work and Research Gap

The literature relevant to this paper spans three connected areas. The first concerns the physical basis of crosswind power generation and the strong dependence of pumping performance on tether force, reel speed, and flight trajectory [1, 4, 7]. Review work has also emphasized that rapidly varying aerodynamics,

gusts, and intermittency are not only flight-control challenges but also electrical-integration challenges [12]. That connection is central here because the EMS ultimately sees the electrical consequence of those flight-layer disturbances rather than the aerodynamics directly. Recent AWES studies have therefore started to address the electrical consequences of pumping-cycle variability and the need for storage-assisted smoothing solutions [13].

The second area concerns electrical interfacing for ground-generation AWES. Ahmed *et al.* [14] develop a simplified dynamic model of a kite generator and dual-converter grid interface, showing grid-connected operation and MPPT adaptation under slowly varying wind assumptions. Their work is relevant because it demonstrates the importance of the generator-side and grid-side conversion chain. However, it does not address hybrid-storage coordination under non-stationary pumping-cycle variability.

The third area concerns EMS architectures for hybrid-storage renewable microgrids. General EMS and microgrid-storage reviews are available in [15, 16], while battery-supercapacitor coordination and supervisory strategies are discussed in [8, 9]. AWES-specific EMS studies remain limited. The closest precursor to the present manuscript is the work of Flores-Martín *et al.* [17], who propose an EMS for a ground-generation AWES microgrid and demonstrate DC-bus regulation and cycle-energy balancing under nominal pumping cycles.

Table 1 positions the present manuscript relative to the most relevant prior work. Relative to [17], the present study does not claim a fundamentally new EMS architecture. It replaces nominal-cycle evaluation with a simulation workflow in which the EMS is tested against variable pumping-cycle profiles generated from the LAKSA/KiteAcrobat environment. The research gap addressed here is therefore the lack of EMS assessment under AWES-derived non-stationary input that preserves both fast intra-cycle content and slower cycle-to-cycle drift.

Table 1 Positioning of the present work relative to selected prior literature.

Reference	Main focus	Input assumption	EMS/storage scope	Limitation relative to this paper
Ahmed *et al.* [14]	Ground-generation kite generator and grid interface	Simplified wind evolution and closed-orbit operation	No AWES-specific hybrid-storage EMS	Does not assess non-stationary AWES-driven storage coordination
Vermillion *et al.* [12]	Review of AWE control research	Highlights intermittency, gusts, and rapidly varying aerodynamics	Not an EMS validation study	Motivates the problem but does not evaluate a microgrid EMS
Flores-Martín *et al.* [17]	EMS for ground-generation AWES	Nominal pumping-cycle profiles	AWES-oriented EMS with DC-bus regulation	Does not inject variable-wind-derived cycle distortions into the EMS assessment
This work	EMS evaluation under variable wind	KiteAcrobat-derived cycle library with randomized cycle selection and amplitude perturbation	AWES-oriented EMS with DC-bus regulation	

3 Simulation Framework and AWES-Derived Input Generation

The paper uses a simulation-based workflow. First, measured wind data are processed and used to drive the LAKSA/KiteAcrobat model of the airborne subsystem. Second, the resulting cycle-resolved AWES-side power traces are segmented, stored, and combined into scenario sequences. Third, those profiles are injected into a Simulink electrical plant model controlled by the Stateflow EMS. Figure 2 summarizes this chain.

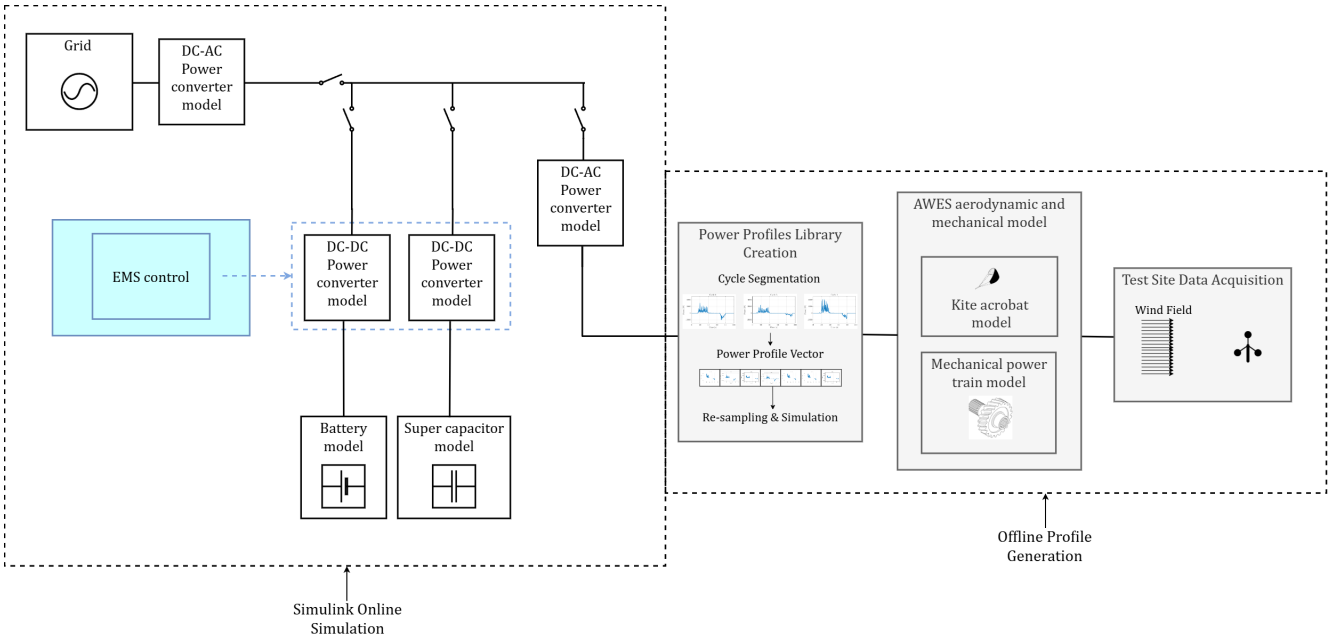

Fig. 2 End-to-end workflow used in the simulation study.

3.1 LAKSA/KiteAcrobat simulation environment

The AWES input profiles used in this paper are derived from the LAgrangian Kite SimulAtors (LAKSA) tool-chain [10]. The underlying two-line KiteAcrobat model represents the kite as a rigid body connected to the ground by two straight, massless, inelastic tethers; tether gravity and aerodynamic drag are neglected, and the constrained six-degree-of-freedom problem reduces to four generalized coordinates handled through Lagrange's formalism [11]. For the present study, this reduced-order structure is appropriate because it preserves the cycle timing and the main force transients needed at the EMS input without introducing unnecessary aerodynamic or aeroelastic complexity, resulting from a more complete description of tether dynamics.

Following the compact formulation of [11], the generalized coordinates are gathered in the state vector

$$\mathbf{x}_s = [\,\phi,\ \gamma,\ \eta,\ \theta\,]^\top, \tag{2}$$

where ϕ and γ orient the plane that contains the tether triangle with respect to the Earth frame, η locates that triangle within the plane, and θ gives the rotation of the kite body frame with respect to the auxiliary frame attached to the tether geometry. The dynamic state advanced by the solver is the extended vector $\mathbf{x} = [\mathbf{x}_s^\top, \dot{\mathbf{x}}_s^\top]^\top$.

The control input is

$$\mathbf{x}_c = [\,\ell,\ \delta\,]^\top, \tag{3}$$

where ℓ is the normalized distance between the ground point and the midpoint of the segment joining the two tether attachment points, and δ represents the steering asymmetry associated with differential line lengths [11]. In the Simulink implementation, the control module updates $\mathbf{x}_c$ from the path-following logic and actuator limits, while the environment, kinematics, aerodynamics, forces, right-hand-side, and post-processing subsystems exchange state and control variables at each time step to reconstruct the kite trajectory and the power-related quantities.

3.2 Derivation of cycle-resolved power profiles

At each time step, the kinematics module computes the kite position, linear velocity, angular velocity, and the associated Jacobians from $\mathbf{x}$ and $\mathbf{x}_c$; the aerodynamic module then forms the apparent wind and evaluates the aerodynamic forces and moments; finally, the forces and right-hand-side modules assemble and integrate the Lagrangian equations of motion [11]. In the KiteAcrobat version used in this work, the reel-out/reel-in velocity is explicitly added to the kite motion when computing the apparent wind, so the force history reflects both crosswind flight and reeling dynamics.

The resulting tether load is converted into ground-side shaft variables through the drum radius, r and the gear-box ratio N. In the implementation used, the tether force F generates a load torque $\tau_{\text{load}} = F \cdot r/N$; inertial and viscous contributions associated with the rotating drivetrain are then added to obtain the total shaft torque τ, and the instantaneous shaft power is computed as

$$P_{\text{shaft}} = \tau\,\omega, \tag{4}$$

with ω the motor angular velocity. The offline LAKSA/KiteAcrobat stage therefore yields the power exchanged at the drum/electric-machine shaft. In the Simulink microgrid, that power is applied at the AWES/electric-machine branch, where the bidirectional machine–converter interface maps the corresponding generated or motoring intervals onto the DC bus.

Short negative excursions within an otherwise generating interval are retained in the exported profiles. They arise when steering or reeling demand temporarily dominates the traction-derived contribution, particularly during rapid path corrections or high-tension transients, and therefore constitute a meaningful stress case for the EMS. These events are also possible during transient operation of ground-generation AWES devices.

3.3 Cycle segmentation and scenario generation

The solver output is exported as a continuous time series and then segmented into full pumping cycles, each one comprising a reel-out interval followed by a reel-in interval. In the dataset considered, each cycle's length varies with time because it is directly coupled to the wind speed. The segmented cycles are stored in a library of N profiles, from which the next cycle is selected during the multi-cycle simulations. Representative examples of the resulting AWES input profiles are shown in Figure 3.

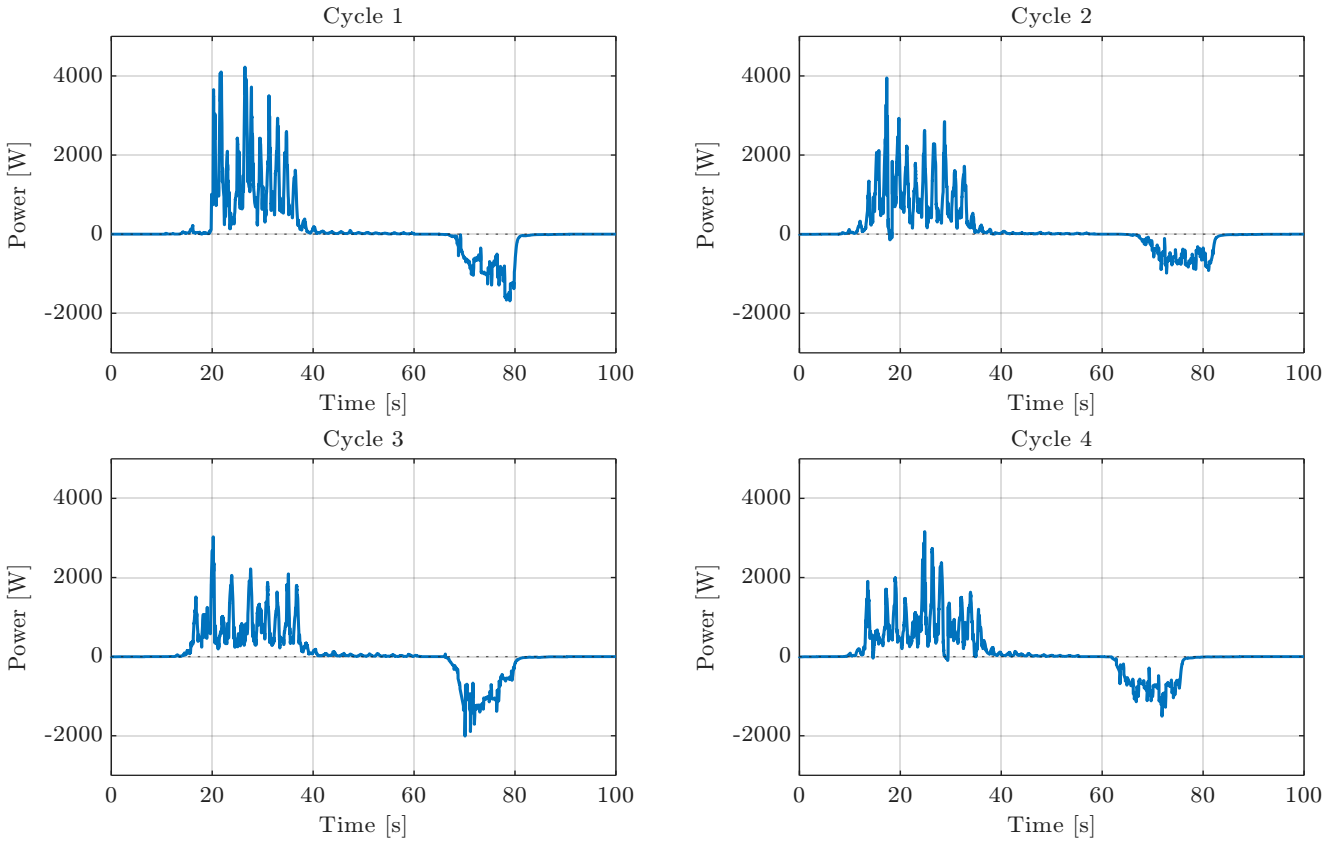

Fig. 3 Representative cycle-resolved AWES input profiles obtained from KiteAcrobat and used in the electrical simulations.

To emulate extended operation with a finite wind record, the multi-cycle simulations draw cycle profiles from this library and apply a per-cycle random amplitude factor υ. This procedure preserves the original intra-cycle waveform while varying the sequence-level operating conditions seen by the EMS.

4 DC Microgrid Model and EMS Design

4.1 Simulated DC microgrid architecture

The AWES-derived input profiles are injected into a simulated DC microgrid comprising an electric-machine interface, a grid-side converter, a supercapacitor branch, a battery branch, and a protection branch. The single-line representation used throughout the paper is shown in Figure 4.

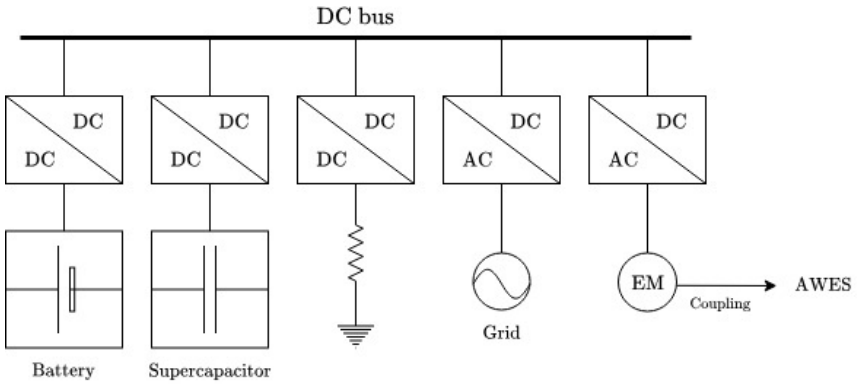

Fig. 4 Single-line diagram of the simulated DC microgrid.

The modeled subsystems and their roles are as follows:

- **AWES/electric-machine branch:** the ground-generation interface is represented by a three-phase electrical machine connected to the DC bus through a bidirectional AC/DC stage. During reel-out, the branch injects power into the DC bus; during reel-in, it absorbs power from it.
- **Grid-side branch:** a grid-tied AC/DC converter exports power from the DC bus. The results reported in this paper concern grid-connected operation only.
- **Supercapacitor branch:** the supercapacitor bank is interfaced through a bidirectional DC/DC converter and is assigned the fast buffering role.
- **Battery branch:** the battery is also interfaced through a bidirectional DC/DC converter and provides slower cycle-level energy correction.
- **Protection branch:** a braking resistor is available as a dissipative path in overvoltage conditions.

4.2 Supervisory EMS objectives and energy coordination

The supervisory EMS has three objectives:

- maintain the DC-bus voltage within admissible limits;
- assign fast intra-cycle power buffering to the supercapacitor branch and slower cycle-level correction to the battery branch;
- preserve continuous grid export despite the strongly time-varying AWES input.

Figure 5 illustrates the intended power-sharing principle over a representative pumping cycle. The grid branch is commanded to deliver a continuous export level, the supercapacitor branch absorbs the fast mismatch between the AWES interface and the grid demand, and the battery branch corrects the residual cycle-average error when the supercapacitor state drifts away from its reference operating point.

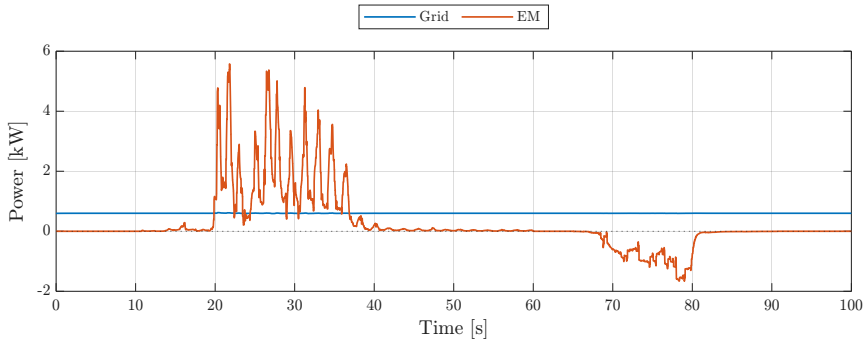

Fig. 5 Illustrative power-sharing principle between the AWES/electric-machine branch and the grid branch during a representative pumping cycle.

For the supervisory relations below, positive P_{EM} denotes net power injected from the AWES/electric-machine branch into the DC bus, and positive P_{grid} denotes power exported from the DC bus to the grid. Positive P_{SC} and P_{bat} denote charging power absorbed by the supercapacitor and battery branches, respectively. Negative storage power therefore corresponds to discharge from storage to the DC bus.

At the end of cycle n, the expected net energy of the next cycle is written as

$$E_{\mathrm{net}}[n{+}1] = E_{\mathrm{reel\text{-}out}}[n{+}1] - E_{\mathrm{reel\text{-}in}}[n{+}1] - E_{\mathrm{grid}}[n{+}1], \tag{5}$$

where $E_{\mathrm{reel\text{-}out}}$ is the energy extracted during reel-out, $E_{\mathrm{reel\text{-}in}}$ is the energy required during reel-in, and E_{grid} is the energy scheduled for export.

The measured deviation of the supercapacitor energy from its reference state is

$$E_{\mathrm{SC,diff}}[n] = E_{\mathrm{SC}}[n] - E_{\mathrm{SC}}[0] = \frac{1}{2}C\left(V_{\mathrm{SC}}[n]^2 - V_{\mathrm{SC}}[0]^2\right), \tag{6}$$

where C is the equivalent capacitance and $V_{\mathrm{SC}}[0]$ is the reference supercapacitor voltage.

The cycle-level energy that the battery must absorb or deliver during the next cycle is then

$$E_{\mathrm{bat}}[n{+}1] = E_{\mathrm{net}}[n{+}1] + E_{\mathrm{SC,diff}}[n]. \tag{7}$$

To avoid unnecessary battery cycling, the supervisory controller applies a deadband:

$$P_{\mathrm{bat}}[n{+}1] = \begin{cases} 0, & |E_{\mathrm{bat}}[n{+}1]| < E_{\mathrm{min}}, \\ \dfrac{E_{\mathrm{bat}}[n{+}1]}{T_{\mathrm{cycle}}[n{+}1]}, & |E_{\mathrm{bat}}[n{+}1]| \geq E_{\mathrm{min}}, \end{cases} \tag{8}$$

where E_{min} is the minimum cycle-energy threshold for battery participation and T_{cycle} is the duration of the selected next cycle.

The instantaneous supercapacitor charging/discharging command follows from the remaining power imbalance:

$$P_{\mathrm{SC}} = P_{\mathrm{EM}} - P_{\mathrm{grid}} - P_{\mathrm{bat}}. \tag{9}$$

In the simulations reported here, the value used in (5) is available from the next selected cycle profile. The paper therefore evaluates the supervisory logic conditioned on that cycle-level information. A separate study of wind-to-energy prediction accuracy is outside the scope of the present manuscript and should not be inferred from the results.

4.3 Local converter roles and protection

The supervisory equations above determine the desired energy allocation. The plant-side converter controls implement that allocation subject to voltage and current constraints.

For the supercapacitor branch, the controller uses a voltage target and current limit consistent with (9). The reference voltage is

$$V_{\mathrm{SC}}^{\mathrm{ref}} = \begin{cases} V_{\mathrm{SC}}^{\mathrm{min}}, & P_{\mathrm{SC}} < 0, \\ V_{\mathrm{SC}}^{\mathrm{max}}, & P_{\mathrm{SC}} \geq 0, \end{cases} \tag{10}$$

and the low-voltage-side current limit is

$$I_{\mathrm{SC}}^{\mathrm{lim}} = \frac{|P_{\mathrm{SC}}|}{V_{\mathrm{SC}}}. \tag{11}$$

With the sign convention adopted above, $P_{SC} \geq 0$ corresponds to supercapacitor charging and $P_{SC} < 0$ to supercapacitor discharge.

The battery branch acts on a slower time scale. Its role is not to absorb every short fluctuation, but to correct the cumulative cycle-level bias represented by (7) and (8). In the reported simulations, the battery current therefore appears only when the cycle-energy correction is needed or when bus-voltage support is required. This is consistent with the intended reduction of unnecessary battery cycling, but the present manuscript does not quantify lifetime benefit and should not claim it beyond this operational interpretation.

The protection branch remains inactive in normal operation. If the DC-bus voltage exceeds a predefined threshold, the braking resistor is commanded to dissipate excess power and prevent overvoltage escalation. A higher threshold is reserved for emergency stop logic in the simulated protection layer.

4.4 Software-in-the-Loop implementation and assessment criteria

The supervisory controller is implemented in Stateflow within MATLAB/Simulink 2024b, while the electrical subsystems are represented in the same simulation environment. This yields a Software-in-the-Loop framework in which the AWES-derived input profiles, the electrical plant, and the EMS interact consistently at system level. This simulation environment offers flexibility during testing, and allows for exploratory analysis of different profiles, generation sources and environmental conditions that might impact performance of the AWES device.

The assessment criteria used in the reported cases are summarized in Table 2: bus-voltage regulation, maintenance of the supercapacitor operating window, continuity of grid export, and clear separation between fast and slow storage roles.

Table 2 Assessment criteria used in the reported simulation cases.

Criterion	Interpretation
DC-bus regulation	V_{DC} remains within the admissible band [0.93, 1.07] p.u. in the reported cases
Supercapacitor operating window	V_{SC} remains within [0.70, 1.30] p.u.
Grid-export continuity	The grid branch remains continuous relative to the strongly variable AWES/electric-machine branch
Storage-role separation	The supercapacitor branch carries the dominant fast fluctuations, while the battery remains inactive in the single-cycle case and intervenes sparsely in the multi-cycle case

A compact conceptual diagram of the EMS logic already used in the project is shown in Figure 6.

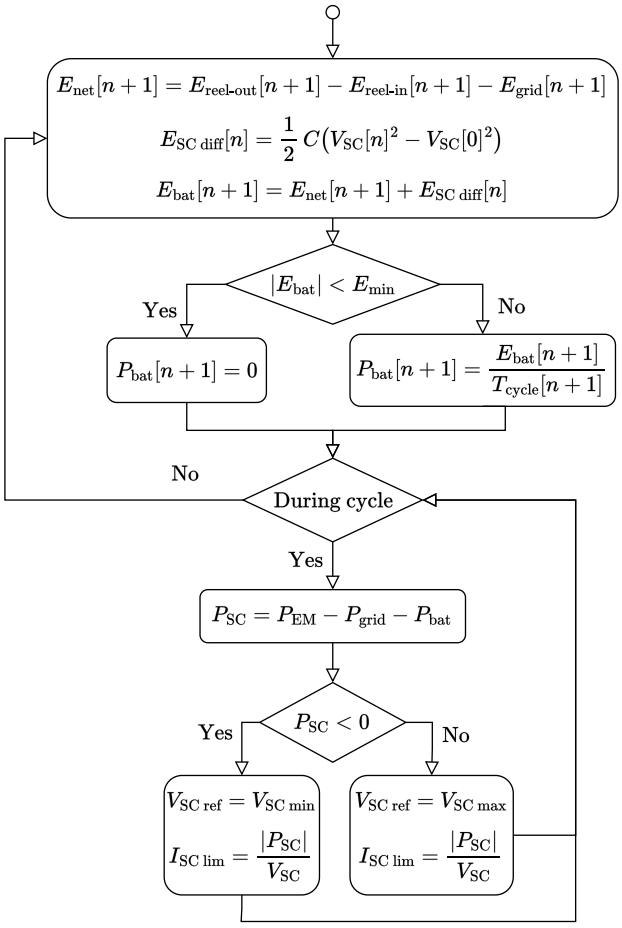

Fig. 6 Conceptual flow diagram of the EMS logic [17].

5 Results and Discussion

The results reported below are limited to the simulation cases already documented in the manuscript: one representative variable-input cycle and one multi-cycle window built from the KiteAcrobat-derived profile library. The discussion therefore remains tied to the available voltage and current traces and to the admissible operating bands defined in Table 2.

5.1 Single-cycle response

Figure 7 shows a representative pumping cycle driven by a variable AWES input profile. The DC bus remains within the admissible range of [0.93, 1.07] p.u., despite the pronounced transients introduced by the AWES/electric-machine branch. The current traces reveal the intended division of labor: the supercapacitor branch responds to the dominant fast excursions, while the battery remains effectively inactive in this particular case. The supercapacitor voltage evolves smoothly and remains inside its admissible window, indicating that the branch has sufficient headroom to absorb the fast mismatch between AWES-side power and grid export.

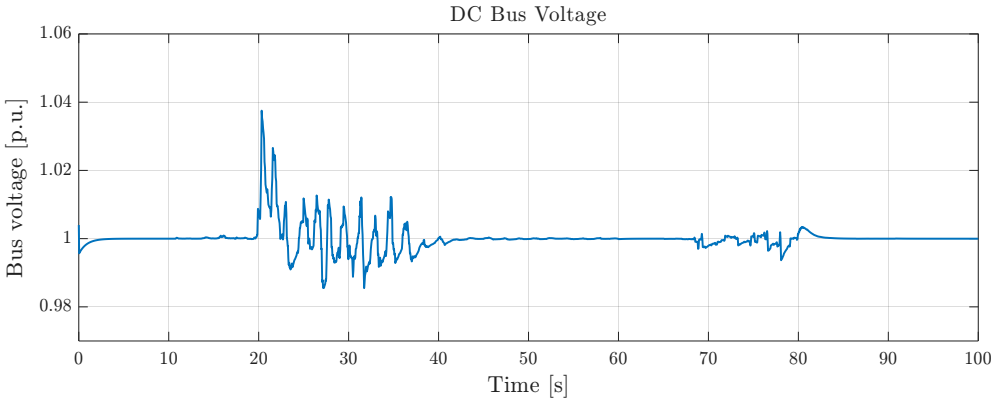

(a) DC-bus voltage during a representative variable-input cycle (p.u., 600 V base).

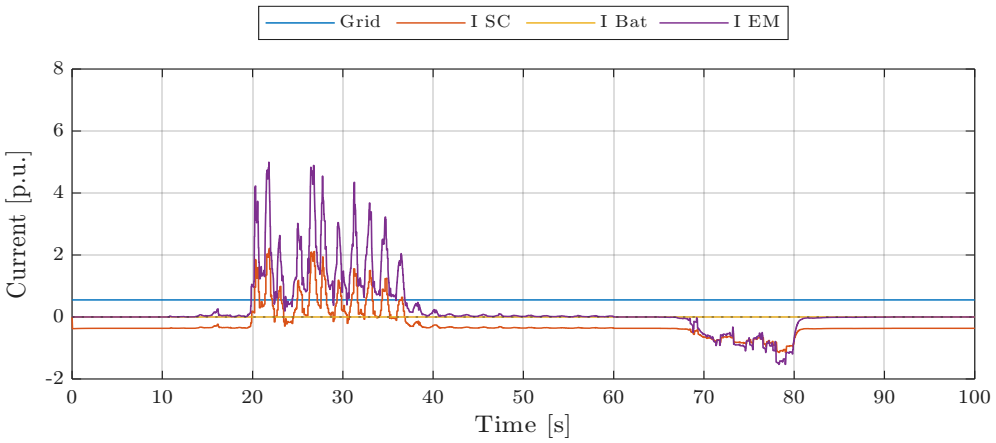

(b) High-voltage-side currents for the grid, supercapacitor, battery, and electric-machine branches.

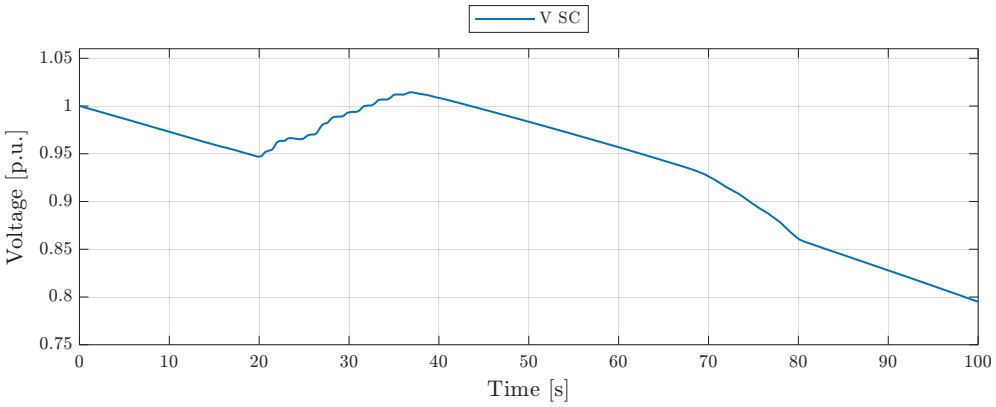

(c) Supercapacitor voltage trajectory over the same cycle.

Fig. 7 Single-cycle simulation results.

The short negative excursions visible in some injected profiles, already illustrated in Figure 3, are consistent with the interpretation given in Section 3: they represent short-duration intervals in which actuation demand locally dominates the AWES-side power balance. In the single-cycle result, those events do not destabilize the bus. Instead, they are absorbed by the supercapacitor branch, which is exactly the type of disturbance rejection the hybrid-storage architecture is meant to provide.

Grid-export smoothing is supported qualitatively by two pieces of evidence. First, the grid branch remains markedly smoother than the AWES/electric-machine branch in Figure 7b. Second, the power-sharing pattern shown in Figure 5 is consistent with the EMS objective of decoupling the grid-side delivery from the fast content of the AWES input.

5.2 Multi-cycle response

Figure 8 extends the analysis to several consecutive pumping cycles. Across this multi-cycle window, the DC-bus voltage remains within the admissible band, which indicates that short-term regulation is preserved even when both the shape and net energy of the injected AWES profiles vary from cycle to cycle. The supercapacitor voltage remains inside its operating window, but unlike the single-cycle case it now exhibits repeated recentering behavior associated with battery intervention.

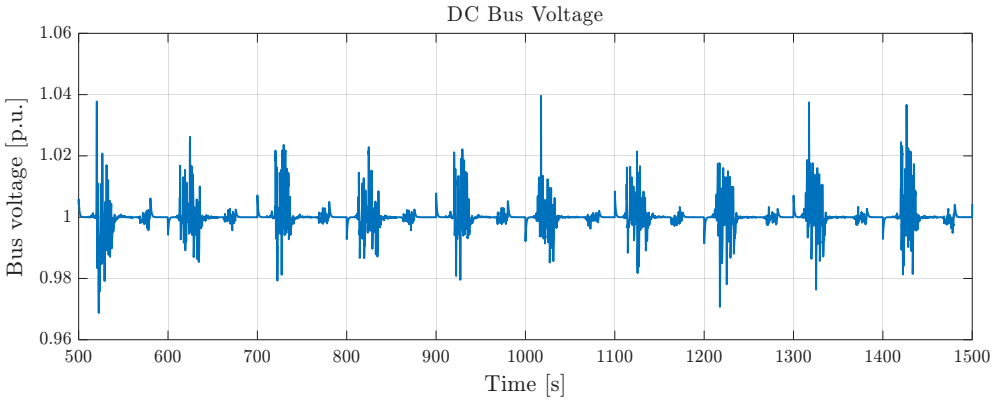

(a) DC-bus voltage across several variable-input cycles.

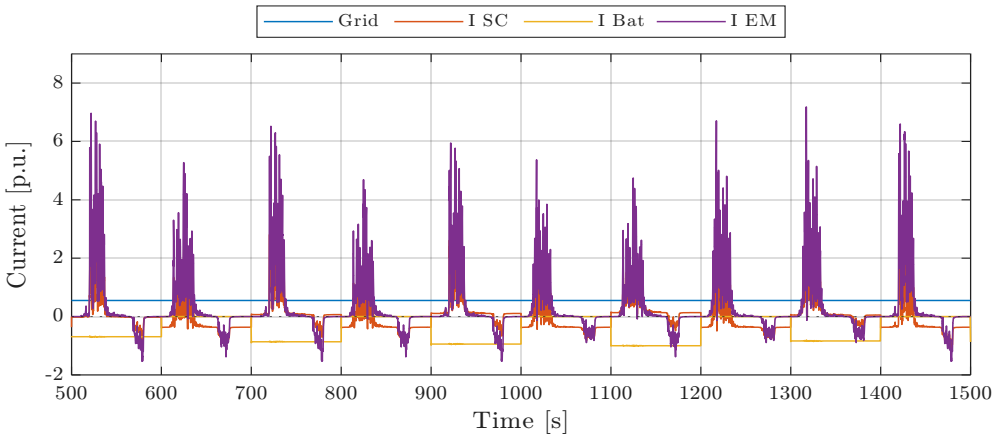

(b) High-voltage-side currents across the same multi-cycle window.

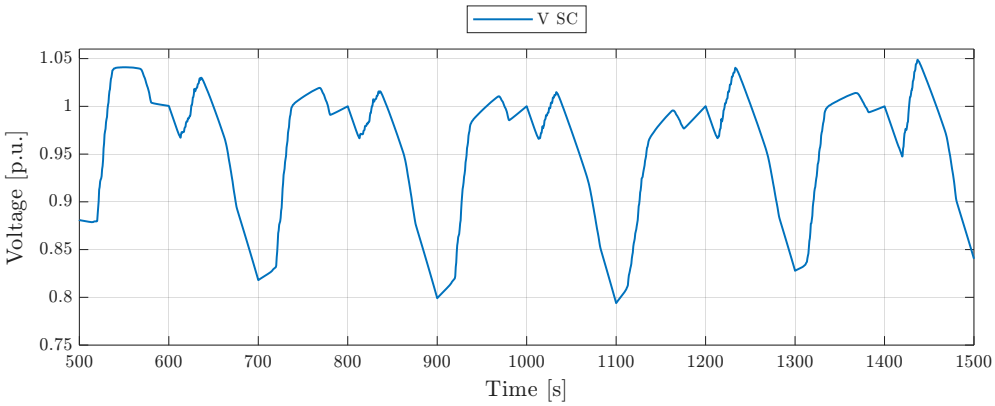

(c) Supercapacitor voltage across the same multi-cycle window.

Fig. 8 Multi-cycle simulation results under non-stationary AWES-derived input.

The current traces in Figure 8b show dense and frequent supercapacitor activity together with comparatively sparse battery participation. This is the expected pattern for the proposed supervisory logic: the supercapacitor remains the primary fast buffer, while the battery acts mainly when cumulative

cycle-level bias would otherwise drive the supercapacitor away from its reference operating region. In that sense, the multi-cycle case is more informative than the single-cycle result because it shows the slower storage branch acting in its intended role.

Table 3 summarizes the main observations supported by the reported cases.

Table 3 Observed behavior in the reported simulation cases.

Case	Main observation
Representative single cycle	DC-bus voltage remains within the admissible band; the supercapacitor carries the dominant fast excursions; the battery remains effectively inactive
Multi-cycle window	DC-bus regulation is preserved across successive variable cycles; the battery intervenes intermittently to recenter the supercapacitor state; fast fluctuations remain concentrated in the supercapacitor branch

6 Conclusion

This paper presented a simulation-based evaluation of an Energy Management System for a hybrid DC microgrid supplied by a ground-generation Airborne Wind Energy System. The distinguishing feature of the study is the use of AWES-derived variable wind pumping-cycle profiles generated with the LAKSA/KiteAcrobat environment and injected into a Software-in-the-Loop electrical model. Through this framework, the EMS is assessed under power profiles that retain both the fast intra-cycle fluctuations of crosswind operation and the slower cycle-to-cycle variation associated with non-stationary wind conditions.

A relevant conclusion of this work emerges when it is compared with prior AWES-oriented EMS studies based on nominal pumping-cycle inputs, particularly the previous work of Flores-Martín et al. [17]. Whereas that earlier study demonstrated the viability of the supervisory architecture under nominal cycle profiles, the present paper shows that the same control philosophy remains effective when the AWES input is made more demanding by variable cycle shapes, actuation-induced short-duration disturbances, and cycle-to-cycle energy drift.

The study also clarifies the practical value of the hybrid-storage architecture for this application. The results support a clear division of labor in which the supercapacitor branch absorbs the dominant fast mismatch between AWES-side power and the grid-side demand, while the battery is reserved for slower corrective action associated with cumulative cycle-level imbalance. For ground-generation AWES, this separation is particularly important because the source variability is structured by the pumping cycle itself and cannot be treated as generic renewable intermittency. The EMS must therefore manage not only average energy imbalance, but also the transient content introduced by maneuvering, reeling, and actuation.

From an electrical-integration perspective, the results reinforce the need to treat ground-generation AWES as a disturbance-rich source rather than as a quasi-steady generator. The contribution of the paper is therefore not only the assessment of a specific EMS implementation, but also the demonstration that AWES-oriented supervisory control should be evaluated with input profiles derived from non-stationary wind conditions, instead of relying exclusively on nominal cycle templates. In that sense, the proposed simulation workflow constitutes a useful intermediate step between conceptual EMS design and future experimental validation, because it preserves the link between airborne dynamics and the electrical disturbances seen by the DC bus.

References

[1] Uwe Ahrens, Moritz Diehl, and Roland Schmehl, editors. *Airborne Wind Energy*. Green Energy and Technology. Springer, Berlin, Heidelberg, 2013. doi: 10.1007/978-3-642-39965-7.

[2] P. Bauer and colleagues. Airborne wind energy: Overview (awesco publication). Technical report, AWESCO, 2016. `https://awesco.eu/publication/bauer-2016-a/bauer-2016-a.pdf`.

[3] Moritz Diehl. Airborne wind energy: Basic concepts and physical foundations. In Roland Schmehl, editor, *Airborne Wind Energy*, Green Energy and Technology, pages 3–22. Springer, Berlin, Heidelberg, 2014. ISBN: 978-3-642-39964-0. doi: 10.1007/978-3-642-39965-7.

[4] M. L. Loyd. Crosswind kite power. *Journal of Energy*, 4(3):106–111, 1980. doi: 10.2514/3.48021.

[5] Volkan Salma, Felix Friedl, and Roland Schmehl. Improving reliability and safety of airborne wind energy systems. *Wind Energy*, 23(2):340–356, 2020. doi: 10.1002/we.2433.

[6] Uwe Fechner. *A Methodology for the Design of Kite-Power Control Systems*. PhD thesis, Technische Universiteit Delft, 2016. doi: 10.4233/uuid:85efaf4c-9dce-4111-bc91-7171b9da4b77.

[7] F. Trevisi, M. Gaunaa, and M. McWilliam. Unified engineering models for the performance and cost of ground-gen and fly-gen crosswind airborne wind energy systems. *Renewable Energy*, 162:893–907, 2020. doi: 10.1016/j.renene.2020.07.129.

[8] W. Jing, C. H. Lai, S. H. W. Wong, and M. L. D. Wong. Battery-supercapacitor hybrid energy storage system in standalone dc microgrids: A review. *IET Renewable Power Generation*, 11(4):461–469, 2017. doi: 10.1049/iet-rpg.2016.0500.

[9] M.-E. Choi, S.-W. Kim, and S.-W. Seo. Energy management optimization in a battery/supercapacitor hybrid energy storage system. *IEEE Transactions on Smart Grid*, 3(1):463–472, 2012. doi: 10.1109/TSG.2011.2164816.

[10] G. Sánchez-Arriaga, A. Pastor-Rodríguez, R. Borobia-Moreno, and R. Schmehl. A constraint-free flight simulator package for airborne wind energy systems. *Journal of Physics: Conference Series*, 1037:062018, 2018. doi: 10.1088/1742-6596/1037/6/062018.

[11] G. Sánchez-Arriaga, M. García-Villalba, and R. Schmehl. Modeling and dynamics of a two-line kite. *Applied Mathematical Modelling*, 47:473–486, 2017. ISSN: 0307-904X. doi: 10.1016/j.apm.2017.03.030.

[12] Chris Vermillion et al. Electricity in the air: Insights from two decades of advanced control research and experimental flight testing of airborne wind energy systems. *Annual Reviews in Control*, 52:330–357, 2021. doi: 10.1016/j.arcontrol.2021.03.002.

[13] R. Joshi, D. von Terzi, M. Kruijff, and R. Schmehl. Techno-economic analysis of power smoothing solutions for pumping airborne wind energy systems. In *Journal of Physics: Conference Series*, volume 2265, page 042069, 2022. doi: 10.1088/1742-6596/2265/4/042069.

[14] Mariam S. Ahmed, Ahmad Hably, and Seddik Bacha. Kite generator system modeling and grid integration. *IEEE Transactions on Sustainable Energy*, 4(4):968–976, Oct. 2013. doi: 10.1109/TSTE.2013.2260364.

[15] W. Su and J. Wang. Energy management systems in microgrid operations. *The Electricity Journal*, 25(8):45–60, 2012. doi: 10.1016/j.tej.2012.09.010.

[16] R. Georgious, R. Refaat, J. Garcia, and A. A. Daoud. Review on energy storage systems in microgrids. *Electronics*, 10(17):2134, 2021. doi: 10.3390/electronics10172134.

[17] Pablo Flores-Martín, Carolina Nicolás-Martín, Osmany R. Pérez-Aballe, Jorge González-García, and David Santos-Martín. Energy management for ground-generation airborne wind energy systems. In *Proceedings of the 23rd International Conference on Renewable Energies and Power Quality (ICREPQ'25)*, Tenerife, Spain, June 2025. ISBN: 978-84-09-66511-2. doi: 10.52152/4546.

Declaration of Use of Artificial Intelligence

AI tools were used during the preparation of this manuscript for language proofreading and for generating helper code used to standardize figure typography and export plots in LaTeX-compatible format. The technical content, engineering interpretation, and final manuscript decisions remained under the authors' responsibility.